Supplementary file

Development of conformation-selective antibodies targeting human SLC15A4

Yalan Zhu[1,#], Xuyuan Zhang[2,#], Qixiang Zhang[1,#], Panpan Sun[2,3,#], Kexin Liu[2,3,#], Xiaohua Nie[2], Junxiao Ma[2,3], Liwei Zhang[2,4], Yina Gao[2], Yong Wang[2], Songqing Liu[2], Ang Gao[1,5,*], Liguo Zhang[2,3,*], Pu Gao[2,3,5,*]

[1] Key Laboratory of Molecular Medicine and Biotherapy, Aerospace Center Hospital, School of Life Science, Beijing Institute of Technology, Beijing, 100081, China

[2] State Key Laboratory of Biomacromolecules, Institute of Biophysics, Chinese Academy of Sciences, Beijing 100101, China

[3] University of Chinese Academy of Sciences, Beijing 100049, China

[4] Department of Nutrition and Health, Beijing Advanced Innovation Center for Food Nutrition and Human Health, China Agricultural University, Beijing 100193, China

[5] Science and Technology Innovation Center, Shandong First Medical University & Shandong Academy of Medical Sciences, Jinan 250000, China

[#] These authors contributed equally to this work

* e-mail: ang.gao@bit.edu.cn; liguozhang@ibp.ac.cn; gaopu@ibp.ac.cn

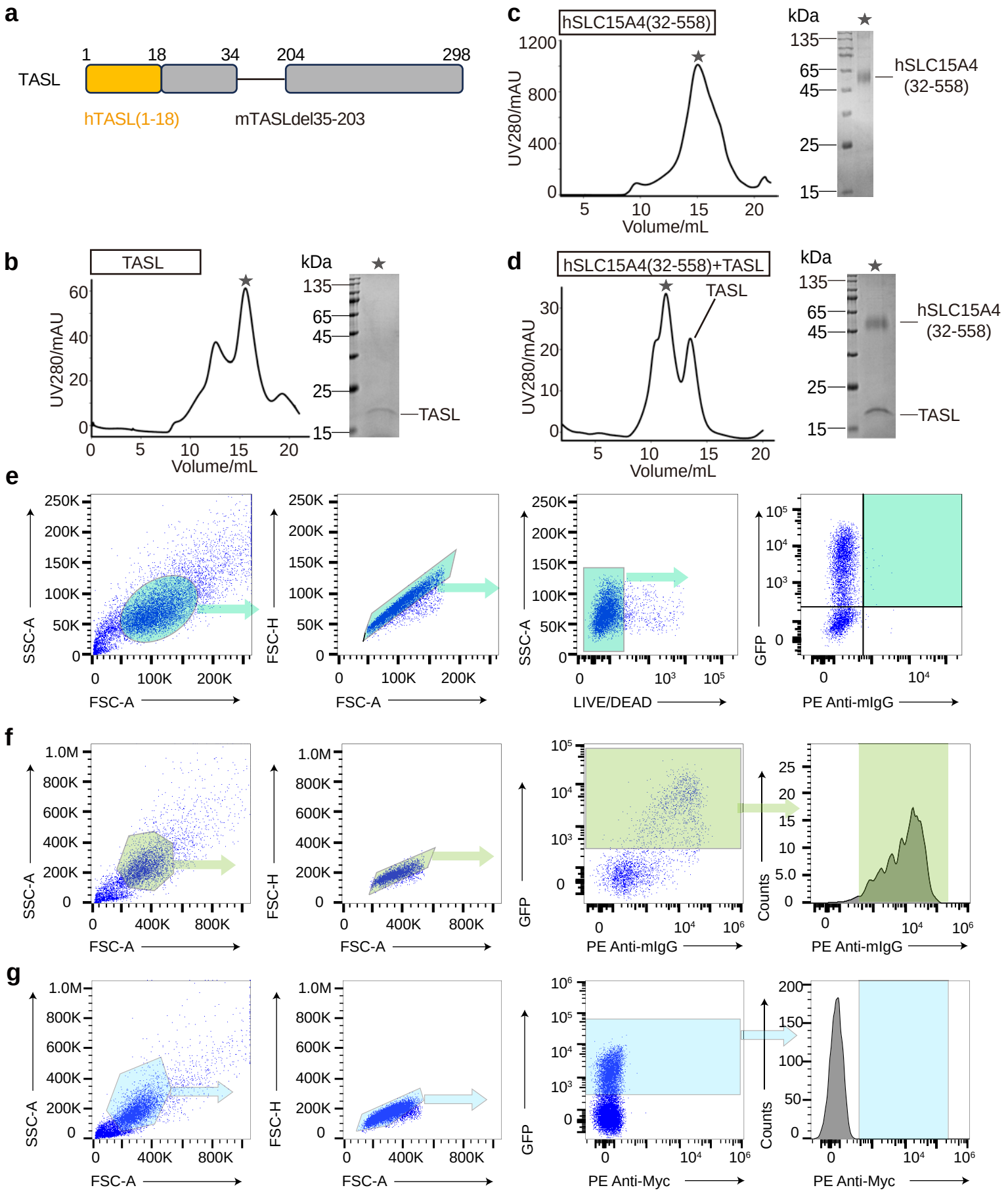

Supplementary Fig. 1 | Protein purification and flow cytometry gating strategy. a, Schematic diagram of TASL construct. The N-terminus of *mus musculus* TASLdel35-203 (mTASLdel35-203) is replaced by N-terminus (aa: 1-18) of hTASL, colored in orange. **b,** Size exclusion chromatography (SEC) profile of TASL and the SDS-PAGE of peak fraction. **c,** SEC profile of hSLC15A4 and the SDS-PAGE of peak fraction. **d,** SEC profile of hSLC15A4-TASL complex and the SDS-PAGE of peak fraction. **e,** Gating strategy of total living cells, SLC15A4 and its mutants is indicated by GFP, while antibody positivity is denoted by mIgG PE (PE goat anti-mouse IgG). **f,g,** Gating strategy of SLC15A4 and its mutant expression cells (GFP^+), histogram showing the binding levels of antibodies (PE goat anti-mouse IgG) or Fabs (PE mouse anti-Myc_tag). (e refers to Fig. 1b, f refers to Fig. 2f and Supplementary Fig. 2a, and g refers to Fig. 3h and Supplementary Fig. 2b) .

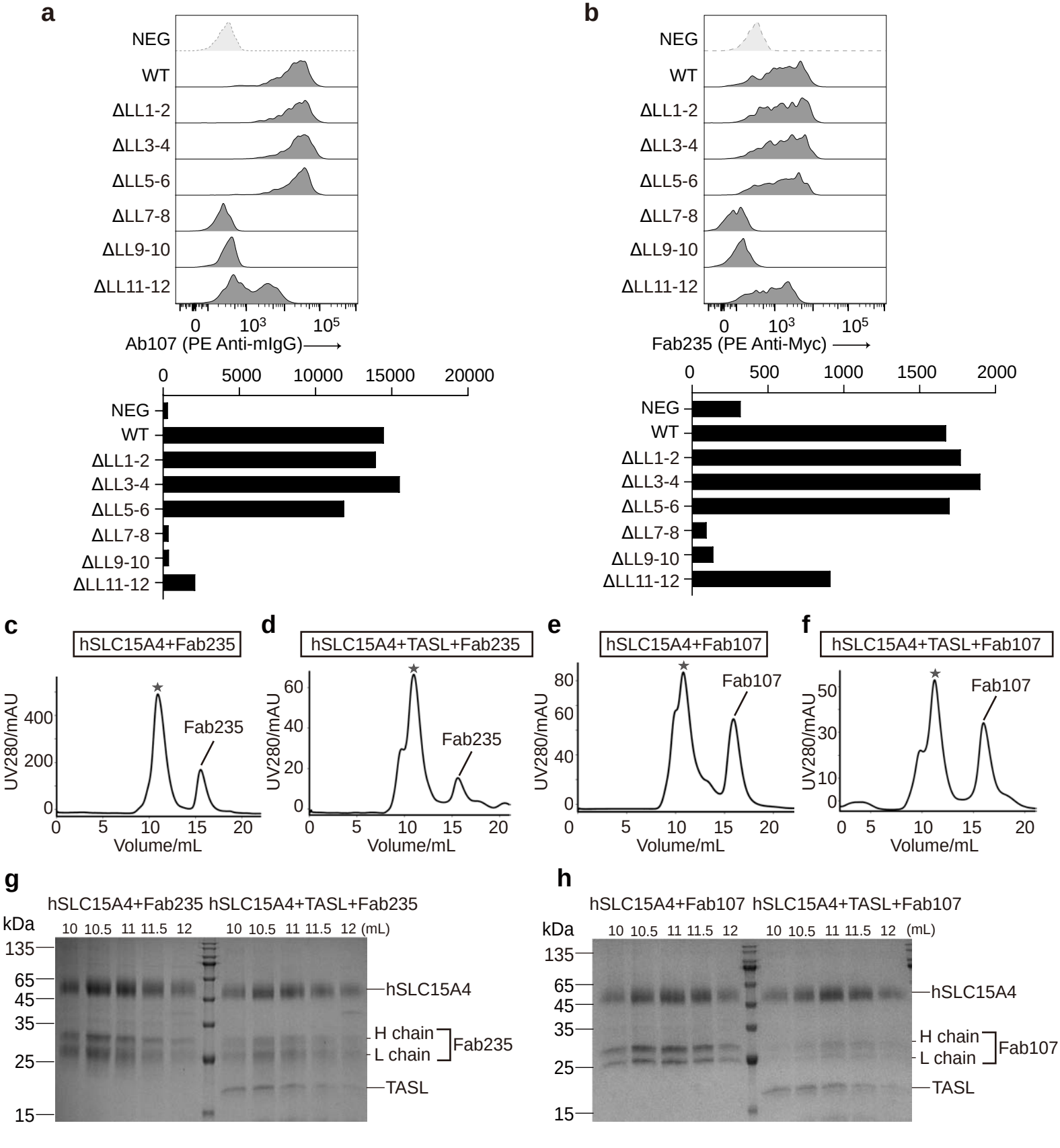

Supplementary Fig. 2 | Binding regions mapping and conformation-specific recognitions of Fab107 and Fab235. a, b, Flow cytometric analyses showing the binding ability of wild type (WT) hSLC15A4 and its mutants (endolysosomal lumen loop substitutions of hSLC15A4) to Ab107 (a) or Fab235 (b). hSLC15A4 mutants used in the experiments are described in Fig. 1c. Data are representative of two independent experiments. **c, e,** SEC profile of hSLC15A4 binding to Fab235 (c) or Fab107 (e). **d, f,** SEC profile of hSLC15A4-TASL complex binding to Fab235 (d) or Fab107 (f). **g,** Coomassie brilliant blue-stained SDS–PAGE gel of hSLC15A4 or hSLC15A4-TASL in complex with Fab235. **h,** Coomassie brilliant blue-stained SDS–PAGE gel of hSLC15A4 or hSLC15A4-TASL in complex with Fab107.

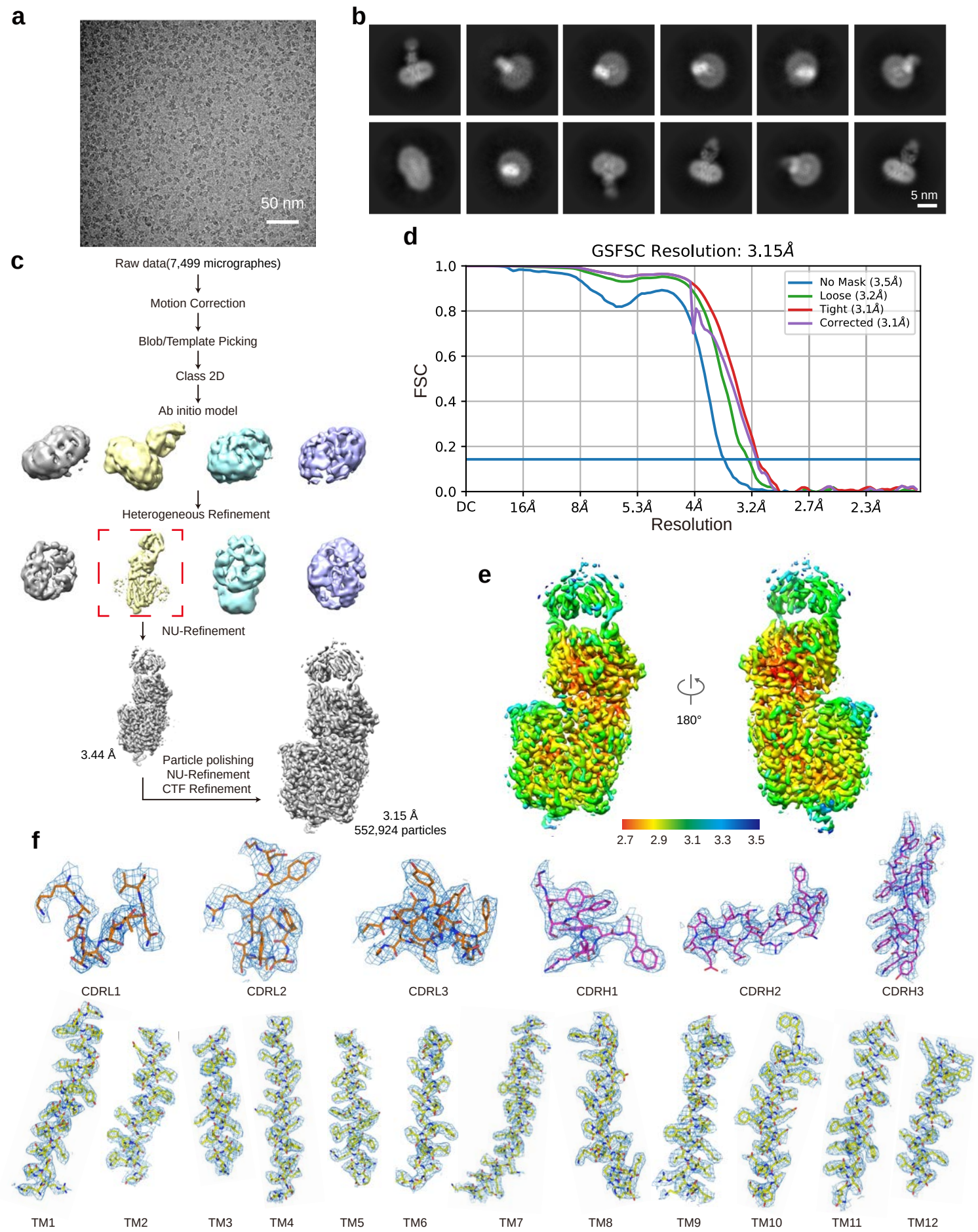

Supplementary Fig. 3 | Cryo-EM data processing of hSLC15A4 bound to Fab107. a, Representative raw micrograph of hSLC15A4-Fab107 complex in nanodisc. **b,** Selected 2D class averages of hSLC15A4-Fab107 complex particles. **c,** Data processing flow chart. **d,** Gold-standard Fourier shell correlation curves of the final reconstruction. **e,** Local resolution distribution of hSLC15A4-Fab107 complex. **f,** Cryo-EM densities of CDRs of Fab107 and transmembrane helices of hSLC15A4 at 7σ.

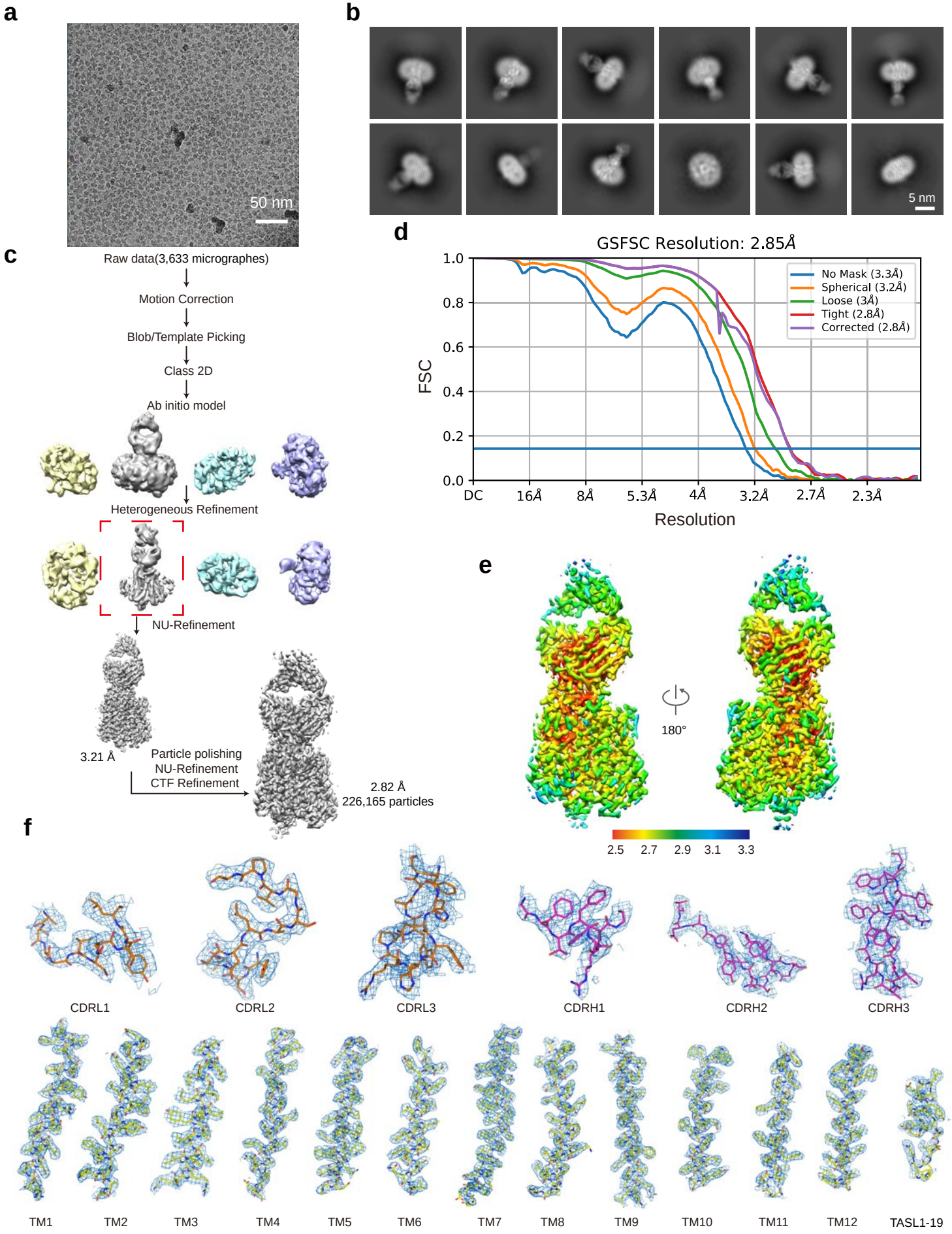

Supplementary Fig. 4 | Cryo-EM data processing of hSLC15A4 bound to TASL and Fab235. a, Representative raw micrograph of hSLC15A4-TASL-Fab235 complex in GDN. **b,** Selected 2D class averages of hSLC15A4-TASL-Fab235 complex particles. **c,** Data processing flow chart. **d,** Gold-standard Fourier shell correlation curves of the final reconstruction. **e,** Local resolution distribution of hSLC15A4-TASL-Fab235 complex. **f,** Cryo-EM densities of transmembrane helices of hSLC15A4, the N terminus (aa:1-19) of TASL and CDRs of Fab235 at 7σ.

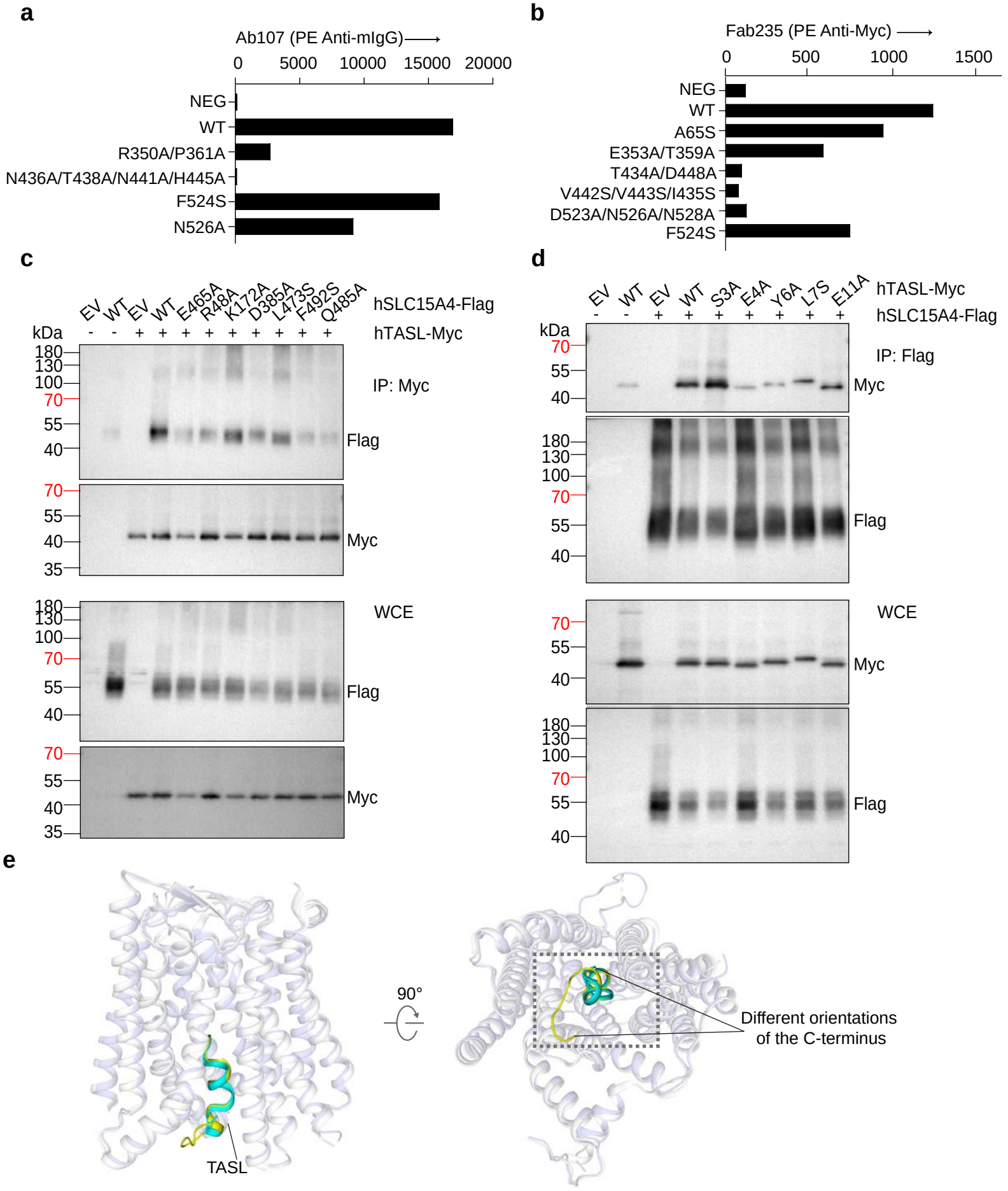

Supplementary Fig. 5 | Mutation analyses of hSLC15A4 and superimposition with reported structures. a,b, Mean fluorescence intensity (MFI) of wild type (WT) hSLC15A4 and its mutants to Ab107 (a) or Fab235 (b). Flow cytometric histograms are shown in Fig. 2f and Fig. 3h. **c,** Immunoblots showing WCE and IP (Myc tag) from Myc-tagged hTASL transiently transfected HEK293T cells co-expressing Flag-tagged hSLC15A4 or its mutants. **d,** Immunoblots showing WCE and IP (Flag tag) from Flag-tagged hSLC15A4 transiently transfected HEK293T cells co-expressing Myc-tagged TASL or its mutants. **e,** Structural superimposition of resolved hSLC15A4-TASL complex (colored in blue) and reported structure (PDB: 8jzu, colored in grey). TASL was colored in yellow and cyan respectively.

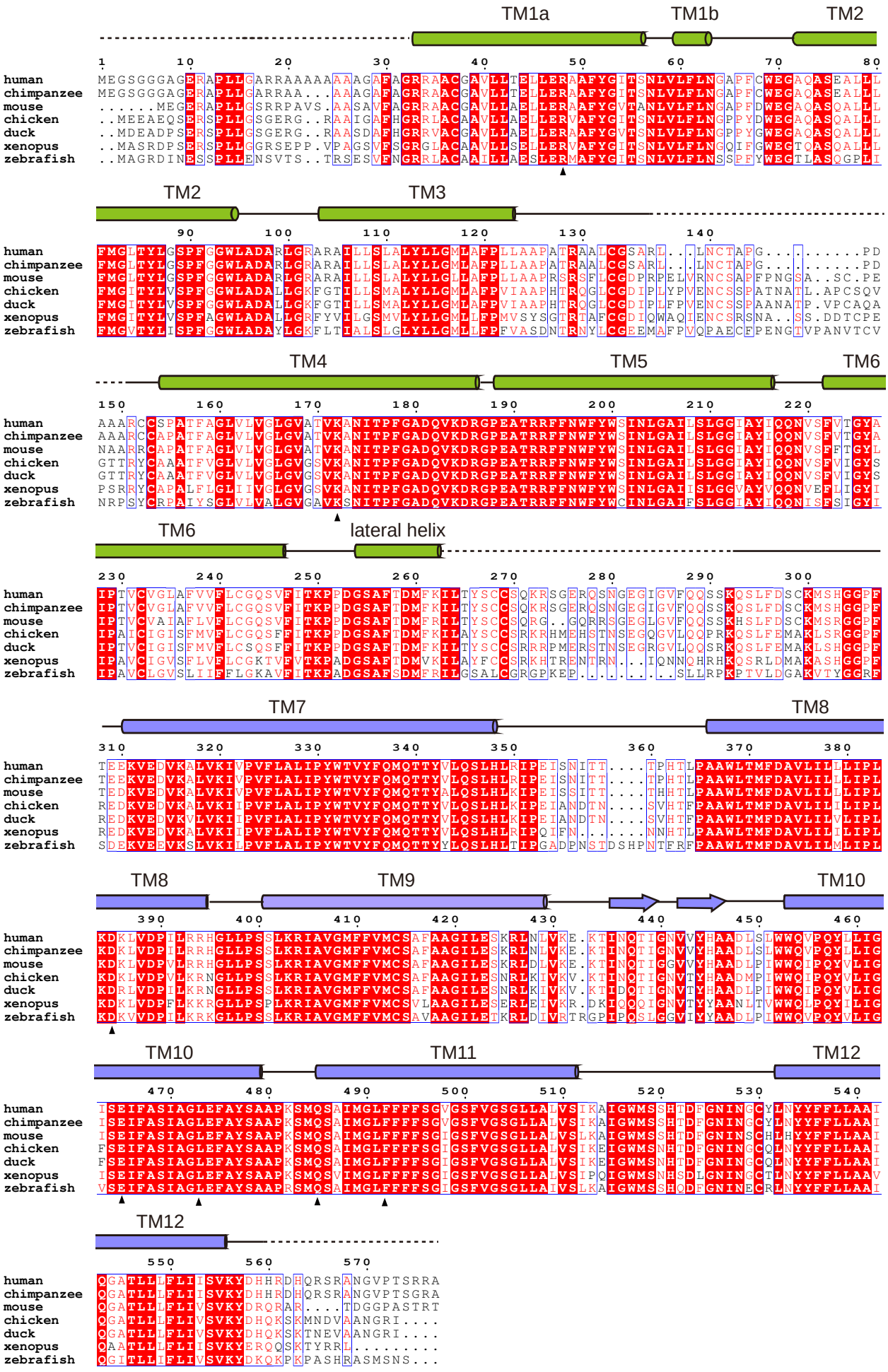

Supplementary Fig. 6 | Sequence alignment of SLC15A4 homologs. The sequences of human SLC15A4 (UniProt entry: Q8N697), chimpanzee SLC15A4 (UniProt entry: H2Q769), mouse SLC15A4 (UniProt entry: Q91W98), chicken SLC15A4 (UniProt entry: A0A8V0ZFZ8), duck SLC15A4 (UniProt entry: A0A493T0R1), xenopus SLC15A4 (UniProt entry: Q68F72) and zebrafish SLC15A4 (UniProt entry: A0A0R4ICA5) were aligned using Clustal-Omega. The figure was generated using ESPript-3.0. The secondary structural elements of hSLC15A4 are indicated above the sequence alignment. Key residues in the TASL-binding pocket of hSLC15A4 are indicated by black triangles.

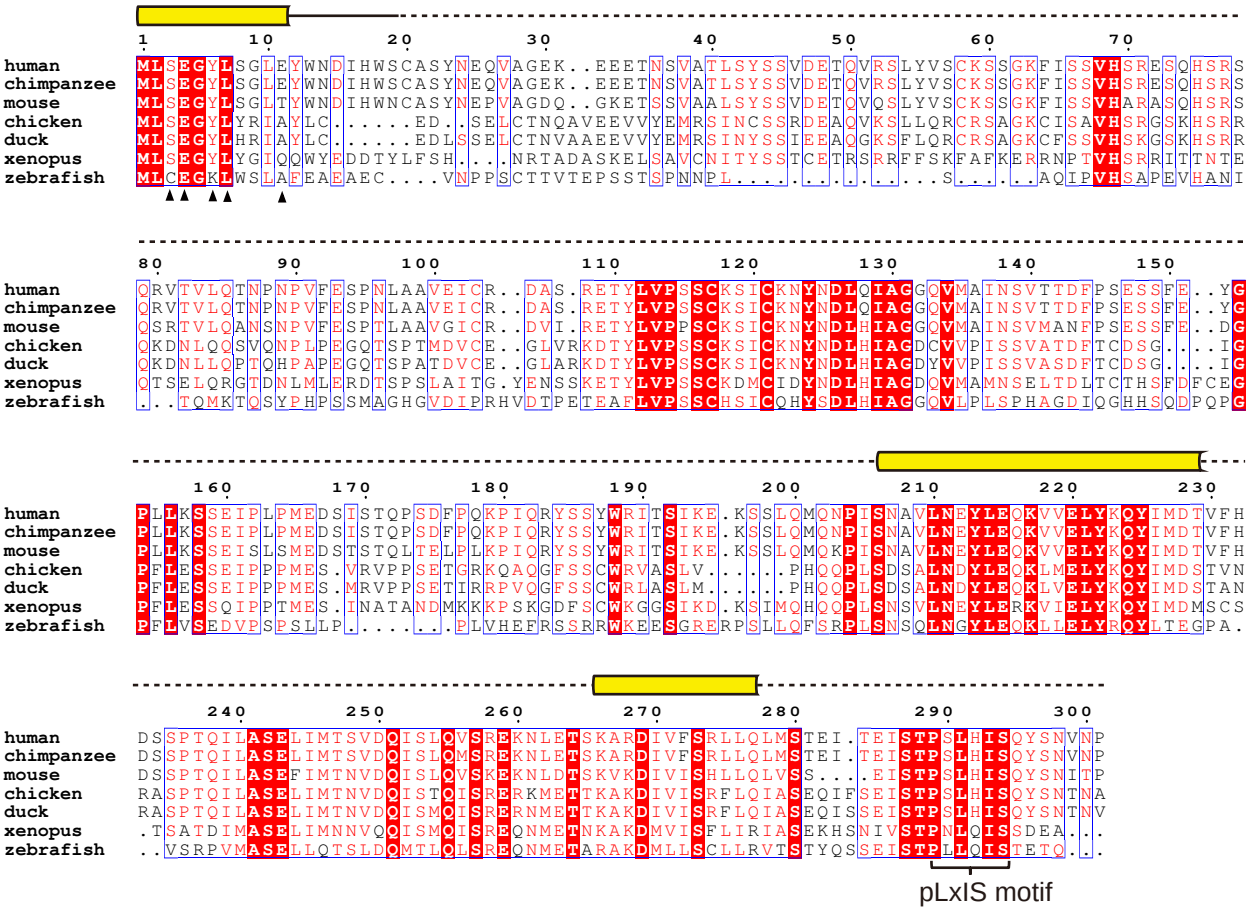

Supplementary Fig. 7 | Sequence alignment of TASL homologs. The sequences of human TASL (UniProt entry: Q9HAI6), chimpanzee TASL (UniProt entry: H2QYF9), mouse TASL (UniProt entry: Q9D3J9), chicken TASL (UniProt entry: A0A1L1RS25), duck TASL (UniProt entry: U3I2N0), xenopus TASL (UniProt entry: A0A974HYV9) and zebrafish TASL (UniProt entry: A0A8M1PYV5) were aligned using Clustal-Omega. The figure was generated using ESPript-3.0. The secondary structural elements of TASL are indicated above the sequence alignment. Key residues in the SLC15A4-binding of TASL are indicated by black triangles.

	hSLC15A4+Fab107 (EMD-60808) (PDB 9IRB)	hSLC15A4+TASL+Fab235 (EMD-60809) (PDB 9IRC)
Data collection and processing		
Magnification	130,000	130,000
Voltage (kV)	200	200
Electron exposure (e–/Å^2)	60	60
Defocus range (μm)	-0.8~-1.5	-0.8~-1.5
Pixel size (Å)	1.0	1.0
Symmetry imposed	C1	C1
Initial particle images (no.)	4,100,012	3,205,673
Final particle images (no.)	552,924	226,165
Map resolution (Å)	3.15	2.82
FSC threshold	0.143	0.143
Map resolution range (Å)	2.7-3.5	2.5-3.3
Refinement		
Initial model used (PDB code)	None	None
Model resolution (Å)	3.4	3.1
FSC threshold	0.5	0.5
Model resolution range (Å)	-	-
Map sharpening *B* factor (Å^2)	-138.8	-90.1
Model composition		
Non-hydrogen atoms	5423	5589
Protein residues	699	726
Ligands	0	0
B factors (Å^2)		
Protein	34.75	119.69
Ligand	-	-
R.m.s. deviations		
Bond lengths (Å)	0.004	0.003
Bond angles (°)	0.565	0.630
Validation		
MolProbity score	1.89	1.93
Clashscore	8.94	11.62
Poor rotamers (%)	0.35	0.17
Ramachandran plot		
Favored (%)	93.90	94.96
Allowed (%)	6.10	5.04
Disallowed (%)	0	0

Supplementary Table 1 | Cryo-EM data collection, refinement and validation statistics.

Clone ID	Chain	Sequence
Fab107	Heavy	QVQLQQPGTELVRPGASVKLSCKASGYSFTRYWMNWVKQ RPGQGLEWIGMVHPSDSETRLNQNFKDKATLTVDKSSSIAY MQLSSPTSEDSAVYYCARWGAYYKYDWDYFDSWGQGTTL TVSS
	Light	DIVMTQSQKFMSTSVGDRVSVTCKASQNVGTNVVWYQQKP GQSPKVLIYSASYRYSGVPDRITGSGSGTDFTLTISNVQSED LAEYFCQQYNNFPYTFGGGTNLEIK
Fab235	Heavy	DVQLVESGGGLVQPGGSRKLSCAASGFTFSRFGMHWVRQ APEKGLEWVAYISSGSSNIYYADTVKGRFTISRDNPKNTLFLQ MTSLRSEDTAMYYCARSTTIIRAFFDYWGQGTTLTVSS
	Light	QIVLTQSPAIMSASLGERVTMTCTASSGVSSSYLHWYQQKP GSSPRLWIYSTSNLASGVPARFSGSGSGTSYSLTISSMEAED AATYYCHQYHRSPWAFGGGTKLEIK

Supplementary Table 2 | Sequences of Fab107 and Fab235.